

Article

# Exploring Building Data from Multispectral and Single-Photon Lidar Systems

Lingli Zhu<sup>1</sup>, Juha Hyyppä<sup>1</sup>, Juho-Pekka Virtanen<sup>2,1</sup>, Xiaowei Yu<sup>1</sup> and Harri Kaartinen<sup>1</sup>

1. Department of Remote Sensing and Photogrammetry, Finnish Geospatial Research Institute, 02430, Masala, Finland; lastname.firstname@nls.fi

2. Department of Built environment, School of Engineering, Aalto University, 02150 Espoo, Finland; lastname.firstname@aalto.fi

\* Correspondence: lingli.zhu@nls.fi Tel: +358 29 530 1100; Fax: +358 9 295 55 211

**Abstract:** This paper investigated building data from multispectral and single-photon Lidar systems. The multispectral datasets from the individual channels and fused channels were explored. The multispectral and single-photon Lidar data were compared across multiple aspects: the data acquisition geometry, number of echoes, intensity, density, resolution, data defects, noise level, and the absolute and relative accuracy. In addition, we explored the performance of the multispectral and single-photon data for roof plane detection in order to investigate the suitability of these data for 3D building reconstruction. The building data from the single-photon and multispectral Lidar systems were evaluated with respect to the reference building vector data with an accuracy of better than 5 cm. The advantages and disadvantages of both technologies and their applications in the urban building environment are discussed.

**Keywords:** multispectral lidar; single-photon lidar; building data; 3D reconstruction

---

## 1. Introduction

Building data have great importance in many applications, such as cartographic mapping, 3D reconstruction and visualization, virtual tourism, urban planning, urban population studies, property taxes, energy demand estimation, assessment of urban heat island effects, and estimation of the building base elevation for flood insurance. Building data can be acquired in different ways: using active sensors or passive sensors. Active sensing integrated with a global navigation satellite system (GNSS) and an inertial measurement unit (IMU) can derive georeferenced 3D building data directly. Therefore, it has become an important means of data acquisition.

Light detection and ranging (Lidar) is a typical active remote sensing technique. Traditional Lidar systems with different modulation techniques can be grouped into two types: continuous wavelength and discrete wavelength systems. Due to many remote sensing applications demanding long-range operation, discrete wavelength lasers with high pulse power have been widely used. Commercial Lidar typically operates on one of the spectra of 1550 nm, 1064 nm, 905 nm, and 532 nm or multiple spectra. Multispectral Lidar systems record the reflection of light on several channels. Each wavelength has its advantages and disadvantages, depending on the target reflectance, background radiation, atmospheric transmission, and eye safety issues [1]. The first operational multispectral airborne laser scanning (ALS) system, Titan, was launched by Teledyne Optech (Ontario, Canada) in January 2015 [2]. The sensor includes three active imaging channels of different wavelengths: 532 nm (visible), 1064 nm (near-infrared, NIR), and 1550 nm (infrared, IR). It is capable of capturing discrete and full-waveform data from all three channels. 3D surface spectral response information sensitive to the emitted wavelengths can be derived day or night from complex environments using a single Lidar sensor [3]. Multispectral ALS can provide data on targets in areas that cannot be measured at a single wavelength (low reflectance at some wavelengths) but that might

be bright at other wavelengths. It gives additional information about the reflectance properties when the response in one wavelength is insufficient to identify a particular target [1].

Commercial Lidar is undergoing a revolutionary evolution from conventional multiphoton Lidar to single-photon Lidar, such as Leica SPL 100. SPL100 splits a single laser beam into 10x10 beamlets. Each beamlet is then imaged onto a pixel in a matching 10x10 array detector. Then, the array detector is input to a timing channel able to record multiple stop events per pixel with an accuracy of a few picoseconds. The use of a 10x10 beamlet array increases the surface measurement rate by two orders of magnitude to 2.2 million multistop pixels per second [4]. SPL 100 has a shorter laser pulse width and lowers the receiver recovery time to, e.g., 1.6 nanoseconds. The low recovery time essentially enables multitarget capabilities. Additionally, this property enables the laser to penetrate vegetation, ground fog, and thin clouds. The SPL100 sensor from Leica/Hexagon uses the frequency-doubled green wavelength of a neodymium-doped yttrium aluminum garnet (Nd:YAG) laser at 532 nm. This visible green wavelength generally exhibits low reflectance values for natural surfaces (15% for soil/dry vegetation and 10% for green vegetation) and is highly transmissive in water [5]. The SPL100 enables acquisition data with higher spatial resolution, larger swath, and greater areal coverage. The point density of the SPL100 sensor is typically 20 points/m<sup>2</sup> at a flight altitude of 4000 m above ground level (AGL). However, except for the advantages of mentioned above, single-photon Lidar is sensitive to background noise. The noise sources include solar backscatter from surfaces, the intervening atmosphere, laser backscatter from the atmosphere, and dark counts from sensitive detectors [4]. However, conventional linear-mode Lidar has multiphoton thresholds and does not record single-photon solar and dark count events.

In contrast to traditional linear-mode Lidar (LML) hardware, single-photon Lidar detectors produce a binary response to impinging photons and therefore do not provide an intensity measure for each detected return [6]. Single-photon Lidar systems employ photomultipliers (tubes, microchannel plates, or silicon) that also respond to single-photon events but with smaller deadtimes, thereby enabling the detection of multiple returns for each emitted laser pulse [4,6]. At a minimum, qualitative interpretation of point clouds is more difficult, while existing processes or workflows that rely on point intensity, e.g., land cover classification, are rendered less effective or inoperable [6].

Building data acquisition is affected by not only the Lidar system and the system operating spectrum but also the interaction between the spectrum and the object surface material. In Finland, typical roofing materials include steel, brick, bitumen, aluminum, and so on. Figure 1 shows the interaction between roofing materials and the spectral reflectance. In general, a highly reflective roof, such as steel roofs or white paint roofs, has a reflectance greater than 50% (50%-90%). The reflectance of concrete, cement, and asphalt is usually between 10% and 35%. Red or brown tile roofs also belong to this category. Brick roofs have a moderate reflectance, typically approximately 40%. Regarding the differences in reflectance at different wavelengths of light, all roofing materials show relatively lower reflectances at wavelengths of 532 nm compared to those at 1064 nm and 1550 nm. Asbestos roofs with a wavelength of 532 nm have a lower reflectance (approximately 10%), while those with a wavelength of 1550 nm show a higher reflectance (approximately 50%). For other materials, the change in the reflectance among these wavelengths is within 10% (see Figure 1).

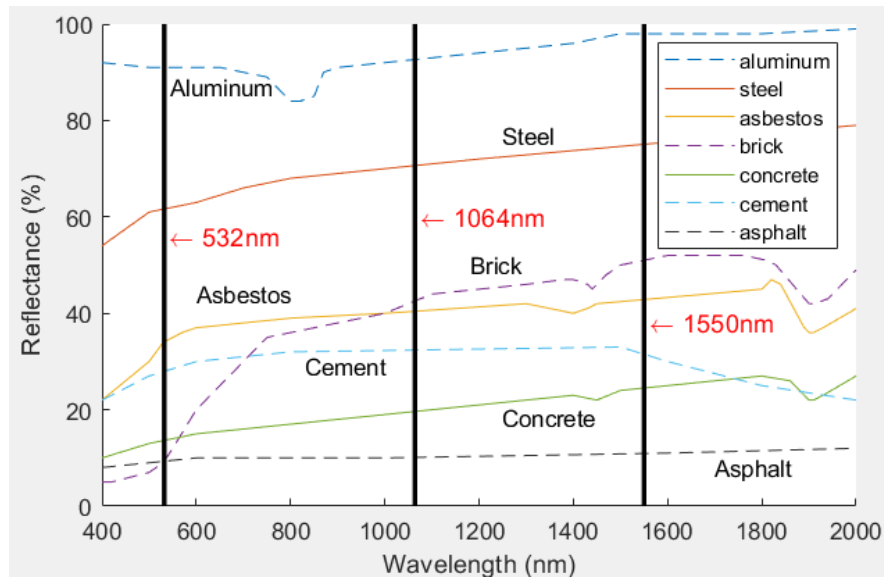


**Figure 1.** The interaction between building roof materials and spectrum.

Materials such as foliage, asphalt and soil reflect or absorb different wavelengths of light in different ways – foliage strongly reflects NIR light but absorbs visible green light, whereas soil responds significantly differently to the same wavelengths. With three independent channels, one for each wavelength, operators can now compare the intensity variations in various surface targets to assist in material differentiation. Typical applications for such systems include 3D land cover classification, vegetation mapping, shallow-water bathymetry, and dense topography [3].

Figure 2 shows that intensity values can be used to distinguish different materials. Vegetation is strongly reflective in the NIR spectrum and slightly less so in the green spectrum. We assume that building materials such as brick and concrete have a similar reflection spectra as cement. The reflection of the building roof has similar NIR and shortwave IR (SWIR) values. In the green channel, its reflection is relatively low. However, the difference is small.

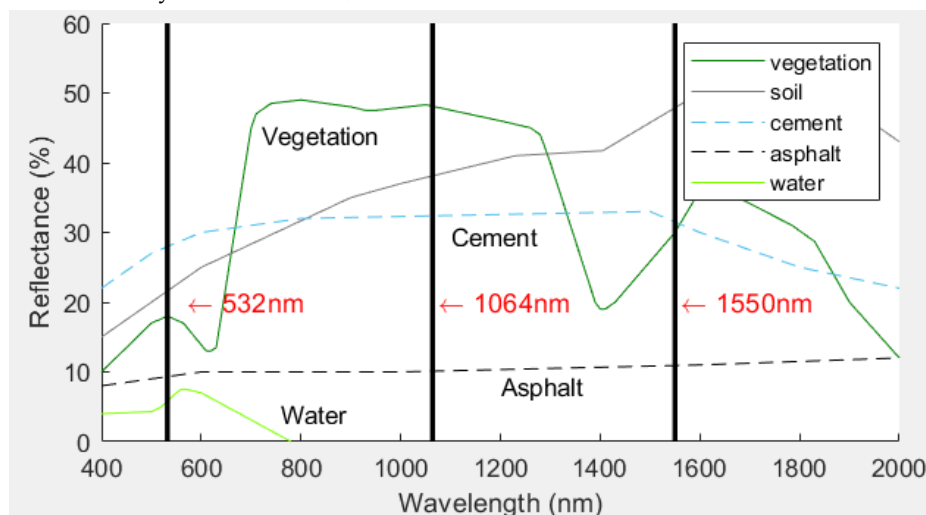


**Figure 2.** Reflection spectra of different materials.

The factors mentioned above, Lidar systems, spectra, and the interaction between spectrum and the surface material, are finally expressed in terms of data characteristics, e.g., the density, resolution, accuracy, and level of detail.

Single-photon and multispectral Lidar data related to vegetation, soil, and water have been investigated by many researchers. However, there is not much information about human-made objects, e.g., building data exploration by means of these emerging Lidar technologies. This paper

aims to study the applicable capability and suitability for 3D building reconstruction and to compare the data from single-photon and multispectral Lidar systems. The multispectral datasets from the individual channel and combined channels were exploited. The multispectral and single-photon Lidar data were compared across multiple aspects: data acquisition geometry, echoes, intensity, density, resolution, accuracy, defects, noise level, and so on. Eight complexes/stylish building roof structures were selected to perform planar roof detection to investigate the levels of detail of the data and suitability for 3D building reconstruction. The accuracy of the buildings from these datasets was evaluated with respect to the reference data.

The contributions of this paper include the following:

- i) The characteristics of echo and intensity information from single-photon and individual channels of multispectral Lidar are surveyed with details;
- ii) Data defects and complementary between channels of multispectral Lidar are studied;
- iii) The suitability of these datasets for 3D building reconstruction is investigated;
- iv) The absolute and relative accuracy of the multispectral and single-photon Lidar building data are examined;
- v) New applications by using echo information for visual enhancement are suggested.

## 2. Related Work

### 2.1. Multispectral Lidar Research

Multispectral Lidar data have been used in many fields, including archeology [7], digital terrain models (DTMs) [8], topographic mapping and land cover classification [9-11], forest environment studies [12,13], map updating [14], water mapping [15], and road mapping [16].

Briese et al. [7] analyzed multispectral ALS data for the prospection of archeological features. The authors noted that the presence of archeological features is significantly related to a specific wavelength. The 1550 nm ALS data exhibited more detailed archeological features than the 1064 nm and 532 nm data. In addition to the sensor's wavelength, the data acquisition time and the actual surface properties are essential for the delineation of archeological features.

Bakula [8] utilized Titan multispectral data to analyze the accuracy of DTMs from three spectral bands. The author found that the mean differences between DTMs were less than 0.03 m.

Wichmann et al. [9] evaluated the potential of an Optech Titan multispectral airborne Lidar sensor for topographic mapping and land cover classification. They claimed that in multispectral datasets, "the class-specific spectral patterns observed in the dataset show similarities to those found in optical imagery." According to the authors' observation, moist surfaces show low reflectance values, and as the surface dryness increases, the reflectance value increases. In addition, the authors also concluded that by providing additional spectral information, the geometrical characteristics of the given dataset are sufficient for geometry-based processing workflows, and there is almost no time gap between the acquisition of the geometrical information of each channel and almost no time gap between the geometrical and spectral information.

Gong et al. [10] classified a scene into seven types using multispectral Lidar data with 556, 670, 700, and 780 nm channels. The overall accuracy was as high as 88.7%. This value was 9.8%–39.2% higher than those obtained using single-channel Lidar data and 4.2% higher than those obtained using multispectral images [10].

Matikainen et al. [14] used multispectral ALS data for land cover classification and map updating. The authors noted that multispectral ALS had advantages in its independence of external illumination conditions when compared to passive aerial imaging and suggested that the multispectral ALS data have a high potential for further increasing the automation level in mapping.

Hopkinson et al. [12] used three independent sensors (1550 nm, 1064 nm and 532 nm) and a single sensor carrying three lasers to investigate multisensor and multispectral Lidar characterization and classification of a forest environment. The authors demonstrated that "when sampling configuration inconsistencies associated with different sensors and platforms are removed by the

integration of multiple lasers into a single sensor, systematic wavelength-dependent differences still occur but are more subtle.”

Karila et al. [16] compared three datasets, specifically, a multispectral ALS dataset, aerial images (AI), and AI plus a digital surface model (AI + DSM) from one-channel ALS, for road mapping. The authors reported that the percentage of roads classified as roads was 78.3% for the multispectral ALS dataset, 68.1% for the AI dataset, and 69.3% for the AI + DSM dataset. It was concluded that “multispectral ALS data are very promising input data for more advanced road detection algorithms.”

Morsy et. al [17] investigated the use of multispectral LiDAR data in land cover classification using two methods. One was that intensity and height images are created from Lidar points and then a maximum likelihood classifier is applied; another was to perform ground filtering and Normalized Difference Vegetation Indices (NDVIs) computation from point cloud. An overall accuracy of up to 89.9% and 92.7% is achieved from image classification and 3D point classification, respectively.

Shaker et. al [18] demonstrated the use of multispectral airborne Lidar intensity data for automatic land-water classification. Two methods were proposed. The first one utilized Gaussian mixture model to separate preliminarily the land and water region based on elevation and intensity histogram; the second one exploited scan line intensity-elevation ratio. An overall accuracy better than 96% was achieved.

## 2.2. Single-Photon Lidar Research

The study of single-photon Lidar data is still in its infancy. An early survey from a hardware development perspective was summarized by Charbon and Regazzoni [5], who proposed single-photon detection and single-photon imaging based on avalanching, especially with single-photon avalanche diodes (SPADs). In 2016, Degnan [4] presented Sigma Space’s single-photon Lidar system and studied topographic and bathymetric mapping using single-photon Lidar data. In addition, a comparison between single-photon and Geiger-mode (GM) Lidar for topographic and bathymetric mapping is performed. The author concluded that GM Lidar appears to be far inferior to single-photon Lidar when probing dense tree canopies. In the same period, many other researchers also published studies:

Stoker et al. [19] evaluated single-photon and GM Lidar data by qualitative testing on 3D terrain, including their relative accuracy and absolute accuracy using 83 ground control points, in order to check if they complied with requirements in the United States Geological Survey (USGS) v1.2 Lidar Base Specifications. The authors concluded ‘while not able to collect data currently to meet USGS lidar base specification, some of this has to do with the fact that the specification was written for linear-mode systems specifically’.

Swatantran et al. [20] evaluated data from a single-photon Lidar instrument, the High-Resolution Quantum Lidar System (HRQLS), for forest canopy structure and ground elevation mapping. They found that “canopy and ground characteristics from single-photon Lidar are similar to discrete return lidar despite differences in wavelength and acquisition periods but the point density of the single-photon Lidar is higher.”

Tang et al. [21] proposed a voxel-based spatial filtering method to remove noise from single-photon Lidar data. The canopy attributes were compared after using different data filtering methods: the spatial filtering method and the conventional histogram binning approach. The result shows that the spatial filtering method retains fine-scale canopy structure detail and has lower errors over steep slopes.

In the last two years, additional related technologies and applications have been addressed:

Jutzi [22] reviewed laser pulse detection with enhanced photon receiver technology from multiphoton Lidar to GM Lidar and single-photon Lidar. The author pointed out that “single-photon Lidar in the visible domain (532 nm) is excellent for bathymetry;” “for GML the penetration capabilities are limited, DTM generation might be difficult;” and “surface reflectance capabilities should be provided by a reasonable radiometric measurement.”

Hartzell et al. [6] introduced a radiometric evaluation of an airborne single-photon Lidar sensor. The authors noted that the high detection probability of the SPL100 sensor is a limiting factor in the quality of radiometric information capable of being extracted from point cloud density measures.

Mandlbürger and Jutzi [23] investigated the possibility of water surface mapping from single-photon Lidar and multispectral Lidar. The findings of the authors are that “for water surface models with a grid spacing of 1-2 m, Single Photon LiDAR often did not deliver enough near water surface points to obtain a gapless model and Multi-Photon LiDAR outperformed Single Photon LiDAR in terms of precision.”

Matikainen et al. [24] investigated land cover classification from single-photon Lidar data. The result showed that single-photon alone is not the most ideal dataset for land cover classification. The highest overall accuracy and the best results for ground-level classes were achieved when multispectral intensity information (infrared and near-infrared) was used.

Mandlbürger et al. [25] compared single-photon with multi-photon full-waveform Lidar. The findings were that the sharpness of the resulting 3D point cloud in the waveform LiDAR dataset is higher, and SPL exhibited moderate vegetation penetration under leaf-on conditions.

To date, related studies on single-photon Lidar data have focused on forest, bathymetry, and terrain modeling. No study has explored building data from single-photon and very few studies from multispectral Lidar systems.

### 3. Materials

#### 3.1. Lidar Systems and Test Area

Our test data are from multispectral and single-photon Lidar systems. Multispectral Optech Titan data were acquired in August 2015 in cooperation with TerraTec Oy (Helsinki, Finland). The flying altitude was approximately 650 m above the ground level. The scanned area included southern parts of the city of Espoo, which is next to Helsinki, and it covers approximately 50 km<sup>2</sup> in total. In this paper, we concentrate on a suburban area in Espoonlahti (see Figure 3). The dataset includes three channels available as separate point clouds (channel 1: IR, 1550 nm; channel 2: NIR, 1064 nm; channel 3: green, 532 nm) [2].

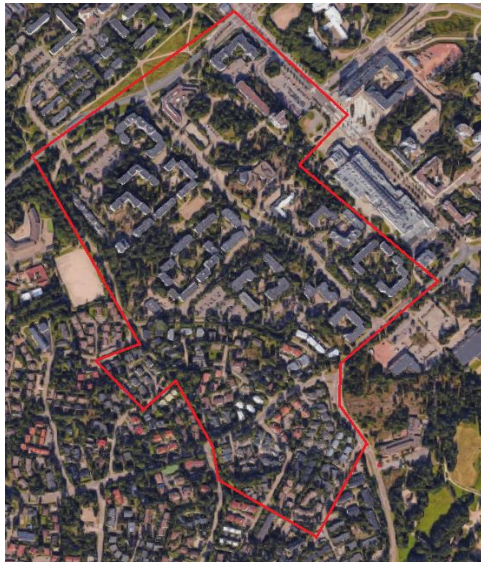


**Figure 3.** Test area in Espoonlahti, Espoo, Finland.

Single-photon Lidar data were collected by a Leica SPL100 sensor (Leica Geosystems, Hexagon, Switzerland), a single-photon airborne sensor, at the flying altitude of 3600 m above the ground level, in August 2018. The system can capture six million measurements per second and penetrate vegetation, ground fog, and thin clouds. It is suitable for large-area mapping. It operates during day

and night, under leaf-on or leaf-off conditions, and in dense vegetation. Table 1 presents data acquisition specifications of multispectral and single-photon Lidar.

**Table 1.** Data acquisition specifications of multispectral and single-photon Lidar

	MSL	SPL
Data acquisition Time	day and night	day and night
Laser Wavelength	532, 1064, 1550 nm	532 nm
Beam Divergence	Channel 1 & 2: $\approx 0.35$ mrad (1/e) Channel 3: $\approx 0.7$ mrad (1/e)	0.08 mrad (1/e <sup>2</sup> per beam, nominal)
Pulse repetition frequency	Programmable; 50 – 300 kHz (per channel); 900 kHz total	60 kHz
Swath Width	0 - 115% of AGL	2000m at 4000m AGL
Field of view	Programmable; 0 – 60° maximum	20°, 30°, 40° or 60° fixed
Point density	Bathymetric: >15 pts/m <sup>2</sup> Topographic: >45 pts/m <sup>2</sup>	Typically 20 points/sqm at 4,000 m AGL
Horizontal accuracy	1/7,500 × altitude	<15cm
Vertical accuracy	<5-10cm	<10cm
Laser range precision	< 0.008 m	
Operational altitude	650 m AGL, all channels	3600 m AGL

\*AGL refers to Above Ground Level

### 3.2. Datasets for Plane Detection

Five datasets were utilized for the study: the three individual channels and the combined-channel multispectral Lidar data and one set of single-photon Lidar data. The average density from the single-channel multispectral data was approximately 8.5 points/m<sup>2</sup> and that of the combined multispectral data was approximately 25.5 points/m<sup>2</sup>. For the single-photon Lidar data, the average density was approximately 48 points/m<sup>2</sup>. Eight complexes/stylish buildings were selected from these datasets. The point densities might vary because of differences in the practical flight speed, flight altitude, weather conditions, and amount of reflection from different objects from the manufacturers' datasheets. Additionally, the point densities in each channel of the multispectral Lidar data might be slightly different due to the interaction between the spectrum and building roof materials. Figure 4 shows an example from the datasets. It can be seen that the single-photon Lidar dataset has more noise than the multispectral dataset.

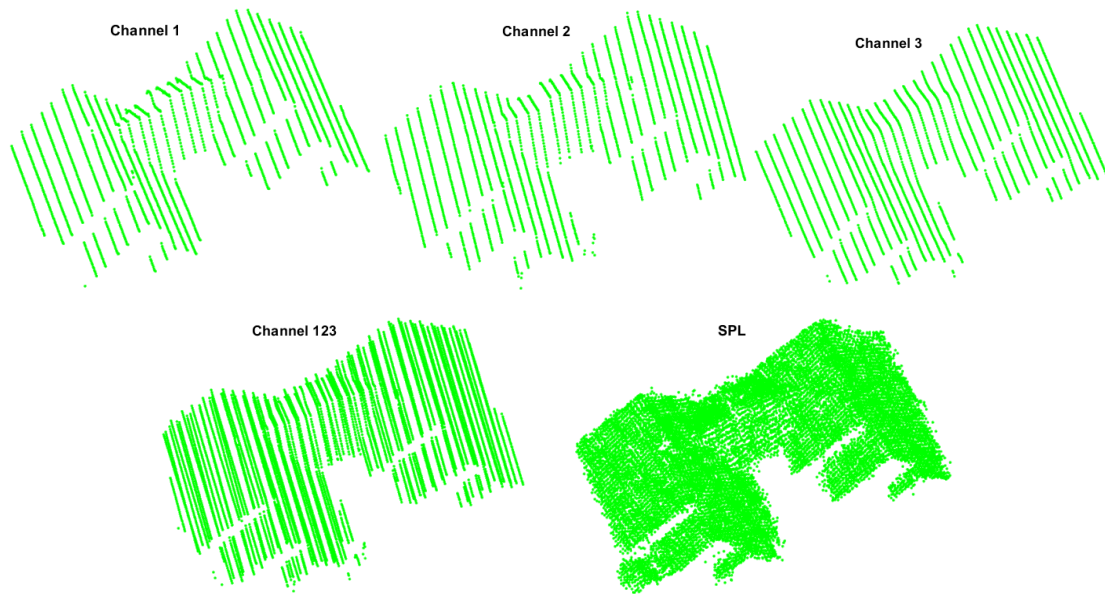


**Figure 4.** Example of a building roof from the different datasets: channel 1, channel 2, channel 3, channel 123, and single-photon Lidar (SPL).

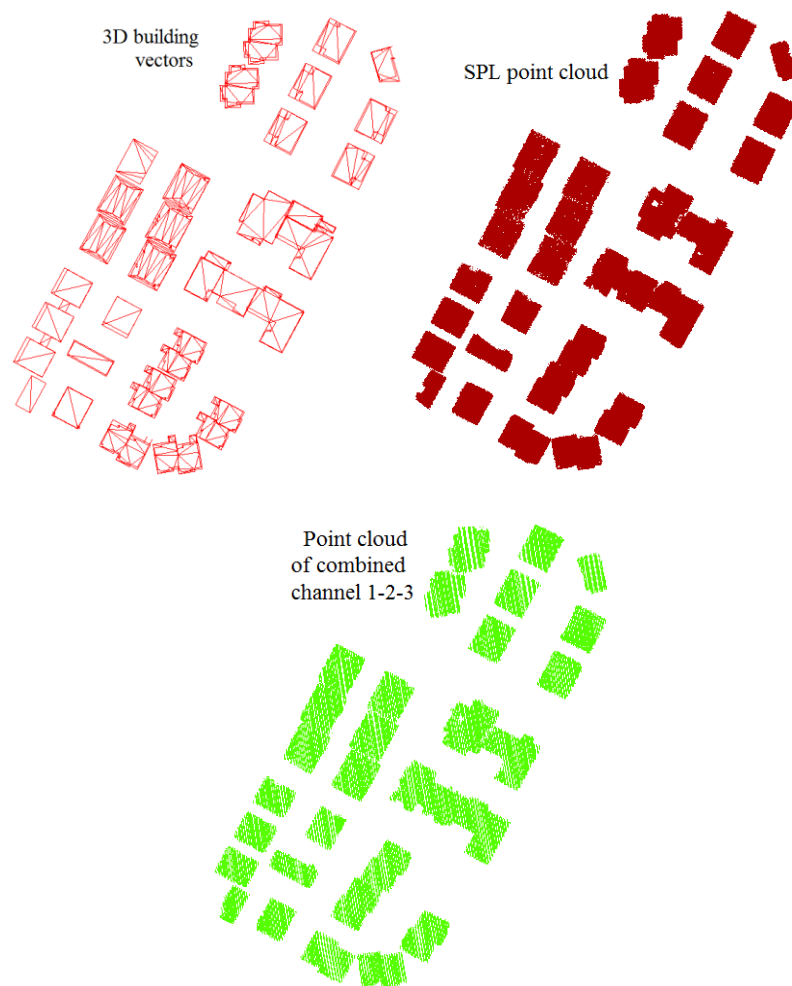
Figure 5 shows the selected buildings with distinctive roof structures. As we can see most of the roofs contain small planar structures with many details. The shapes of the roofs are not irregular. How well they are represented by the individual channel and combined channels from the multispectral and single-photon Lidar datasets will be investigated.



**Figure 5.** Selected complex buildings with small details.

### 3.3. Datasets for Building Accuracy Evaluation

For the reference data, we acquired 3D building data with level of detail 3 (LoD3) from the City of Espoo. The data were provided in two formats: vector (.dwg) and 3D building model (.fbx). These vector models were in the ETRS-GK25 coordinate system and the N2000 height system. The positional and height accuracy of the reference data has been verified to be less than 5 cm after comparing the vector data with the high accuracy ALS point cloud. The single-photon Lidar data were in the ETRS-TM35FIN coordinate system with an ellipsoid projection, while the multispectral Lidar data were acquired in the ETRS-TM35FIN coordinate system of and the N2000 height system. To evaluate the accuracy of these data, we transform the single-photon and multispectral Lidar data to the ETRS-GK25 N2000 coordinate system to match the reference data. We first transformed the single-photon Lidar data from ETRS-TM35FIN Ellipsoid to ETRS-TM35FIN N2000, then to ETRS-GK25 N2000, by a professional application developed by the National Land Survey of Finland [26]. We transform the multispectral Lidar data from ETRS-TM35FIN N2000 to ETRS-GK25 N2000 in one step. Twenty-eight buildings were selected from five datasets, namely, the single-photon Lidar data, combined multispectral Lidar data, channel 1 data, channel 2 data, and channel 3 data, for accuracy evaluation. Figure 6 shows the different datasets: the reference data, the single-photon Lidar data, the individual multispectral Lidar channel data, and the combined data.



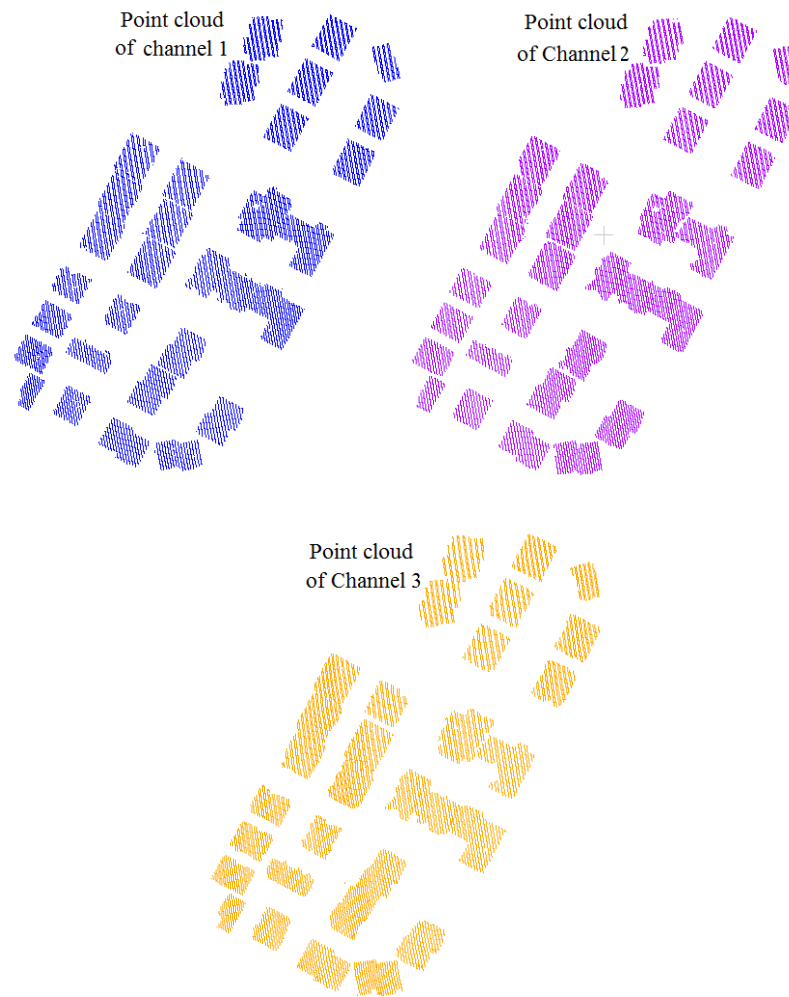


**Figure 6.** Evaluation datasets.

## 4. Methods

As we have mentioned, different Lidar systems, different spectra, and the interaction between the spectra and the object surface materials are finally expressed in the following characteristics: the data acquisition efficiency, accuracy, geometry, number of echoes, density, intensity, and resolution (level of detail), data defects and noise level. We explore the multispectral and single-photon Lidar data in terms of the above aspects. Additionally, the roof planes from complex buildings are detected by applying the maximum likelihood estimation sample consensus (MLE-SAC) method on the multispectral and single-photon Lidar data. Thus, the usability of the data for 3D building reconstruction was analyzed.

### 4.1 Aspects of study

The data acquisition geometry refers to the angles of the sensors with respect to the nadir view. The look directions of the channels in multispectral Lidar are: channel 1:  $3.5^\circ$  forward, channel 2: nadir, channel 3:  $7^\circ$  forward. The operational mode of the single-photon Lidar system is oblique with a fixed angle of  $20^\circ$ . The visibility of building roofs and facades will be observed from single-photon and multispectral Lidar data.

The backscattered echo contains rich information. The echo from flat terrain is simply a replica of the original laser pulse, but over vegetated and built-up areas the backscattered echo is often rather complex [27]. The number of echoes of each point in the individual channels of the multispectral and single-photon Lidar will be statistically counted and compared. Such information is beneficial for object detection/classification.

The intensity value is useful for interpreting the Lidar spatial information. The intensity indicates the strength of the optical backscattered signal. It is related to the following factors: i) target's reflectance at the given laser wavelength; ii) target characteristics such as roughness; iii) the lidar cross-section; iv) on sensor-target geometry parameters including range and incidence angle [28]. Multispectral Lidar measures intensity value from each laser beam. However, SPL 100 doesn't produce intensity data, instead, in the form of pulse-width. In this study, we utilize histograms to analyze the ranges and distribution of intensity values in each channel of multispectral Lidar. Besides, the intensity value for object classification is explored. Data from each channel are tested.

The point density refers to the number of points in one square meter. It is related to the level of detail of a scene. The density variations in the data from different systems might be caused by different data acquisition geometries, flight heights, flight speeds, and interactions between the different spectra and materials. Density variations in the individual channel of multispectral Lidar data might be affected by the characteristics of the spectra interacting with different materials. Several building roofs are selected randomly for the point density investigation. It aims to investigate if there exists a regular pattern that a certain channel in multispectral Lidar can capture more building points than the other channels. Also, the point density between the combined channel data of multispectral Lidar and single-photon data is compared.

Due to the characteristics of the interaction of different wavelengths with the roof materials and different looking angles of Lidars, data acquired from one channel might have defects, but one from the other channel might be complete. We compare and investigate the level of details and completeness of the building data from the individual channels, the combined channels of multispectral Lidar, and single-photon Lidar data.

Noise in Lidar data is typically from i) dark counts from the sensitive detectors, ii) laser backscatter, and iii) solar backscatter. Conventional Lidar has multiphoton thresholds for accepting the solar and dark count events, while single-photon has only one single-photon threshold. From our datasets, the noise level will be visually observed by selecting some building roofs from each channel of multispectral Lidar and single-photon Lidar data.

#### 4.2. Plane Detection

Eight stylish/complicated buildings were selected as test data. The "complication" refers to small details and structural changes in the building data. These data were acquired from five data sources: the individual multispectral point cloud channels (channel 1, channel 2, and channel 3), the combined multispectral point cloud channels, and the single-photon point cloud data. In each dataset, the building roofs and ground are segmented. In our case, we focus on the 3D building roofs. Therefore, to avoid errors from automated building extraction, we selected the test buildings visually to ensure building completeness. The roof planes are detected by utilizing the MLESAC method.

- MLESAC method

The MLESAC method originated from the random sample consensus (RANSAC) method. The RANSAC method iteratively estimates the parameters of a mathematical model and tests the parameters to acquire the maximal number of correspondences with an outlier below a given threshold. The MLESAC method is an improvement on this algorithm. It takes the distribution of the outliers into account by utilizing the log-likelihood of the solution. The difference between the RANSAC and MLESAC methods can be described from the following cost functions [29]:

$C_1 = \sum_i f(e_i^2)$ , where  $f(e_i^2) = \{0, \text{ if } e^2 < T^2; \text{ constant, if } e^2 \geq T^2$ ,  $C_1$  is the RANSAC cost function;

$C_2 = \sum_i f(e_i^2)$ , where  $f(e_i^2) = \{e^2, \text{ if } e^2 < T^2; T^2, \text{ if } e^2 \geq T^2$ ,  $C_2$  is the MLESAC cost function;

$e_i$  is the error. A data point is an inlier when  $e^2 < T^2$ ; a data point is an outlier when  $e^2 \geq T^2$ .

#### 4.3. Comparison of the Building Data with Respect to the Reference Data

We selected 28 buildings from each dataset and compared the building data from the multispectral and single-photon Lidar systems with the 3D vectors of buildings provided by the City

of Espoo. The mean distance and the standard deviation are estimated. We employed the following equations to estimate the mean distance and the standard deviation:

$$\underline{Y} = \frac{\sum_{t=1}^n Y_t}{n} \quad (1)$$

$$SD = \sqrt{\frac{\sum_{t=1}^n (Y_t - \underline{Y})^2}{n}} \quad (2)$$

where  $Y_i$  is the distance from point  $t$  ( $t = 1, 2, 3, \dots, n$ , where  $n$  is the number of points) in the compared point cloud to its nearest neighbor in the reference point cloud.  $\underline{Y}$  is the mean distance.  $SD$  is the standard deviation.

We also evaluated the relative accuracy of the multispectral and single-photon Lidar data with respect to the building data from channel 1. We chose channel 1 as the reference data because it is more accurate than the original reference data.

## 5. Results

### 5.1. Comparison of the Data acquisition Geometries

Figure 7 shows the building facades from single-photon and multispectral Lidar, respectively. It can be seen that in high buildings, the facades are partly visible from both systems. And more details are presented in single-photon data. It can be interpreted that single-photon Lidar has a bigger oblique angle when operating and produces a higher density of point cloud compared to multispectral data. For low buildings (e.g. one or two floors), although both systems are operated in oblique mode, building facades are missing from both data.

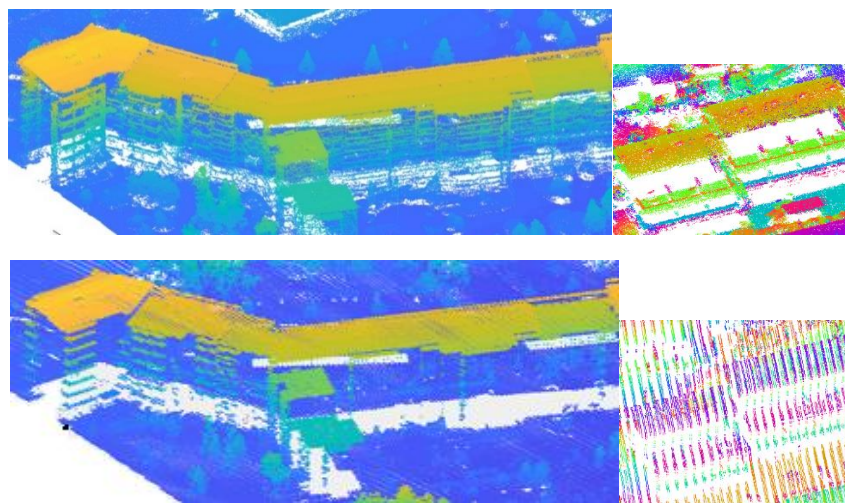


**Figure 7.** Visualization of the building facades from i) the single-photon Lidar system (upper) and ii) the multispectral Lidar system (lower). The colors are randomly presented.

### 5.2. Comparison of the Echo Information from the Multispectral and Single-Photon Lidar Data

In our datasets, the maximal numbers of return echoes in the single-photon and multispectral Lidar are the same, that is, four returns. However, echo information from multispectral Lidar is different from single-photon Lidar. Also, it varies in the different channels of multispectral Lidar. Table 2 illustrates the echo information from one echo to four echoes in multispectral and single-photon Lidar. In Table 2, 'Percentage' refers to the percentage of the number of points in the different number of echoes out of the total number of points in each channel. In single-photon data, 88.01% of points have only one echo while a few points contain four echoes. In multispectral data, most of the points are from one or two echoes. From Table 2 can be seen, channel 2 has 10.77% of points with four echoes, while channel 3 has only 0.52% of points with four echoes. In general, the points with

more than two echoes typically belong to forests/vegetation. From the dataset of channel 3, there was less vegetation acquired than from the other channels. Furthermore, our study shows that building roofs typically have one or two echoes. For building points with two echoes, the first echo is from the edge of the roof, and the second echo is from the base of the building. It is because one laser pulse in the edge of a roof splits into two. One hits on the edge of the roof; another hits the ground. Thus, two echoes are returned. An example from channel 1 data is shown in Fig. 8. Fig. 8 (a) shows the point cloud with one echo. For example, bare ground, most of the roof points, top of vegetation, and so on, belong to this category. Point clouds with two, three, and four echoes from channel 1 are shown in Fig. 8 (b), (c), and (d), respectively.

Building points with one or two echoes were observed from channel 1, channel 2, and single-photon data. However, channel 3 shows different from the other datasets. Some building features were also observed from the points with three echoes. Fig. 9 shows the case. The red points with three echoes from channel 3 were overlapped with the point cloud from the scene. Concerning the single-photon data, 99.57% of it was from the first and second echoes. 0.43% of the points have three echoes. Only a few points have four echoes. Single-photon Lidar split one laser beam into 10x10 beamlets. It has a short pulse and a short return time. Such a work mechanism of single-photon Lidar results in fewer points in the third and the fourth echoes. In single-photon Lidar data, all buildings have one or two echoes, and most of the vegetation has one or two return echoes. For vegetation investigation, more details about echoes from canopies can be found from Brown et. al (2020) [28]. They pointed out that "Of the thirty sampled tree canopies, only 22% of SPL100 emitted pulses had multiple returns, as compared to 87% for the Titan."

**Table 2. Echo information in different systems and different channels**

System or channel	Number of the points	With one echo (Percentage)	With two echoes (Percentage)	With three echoes (Percentage)	With four echoes (Percentage)
Channel 1	1 588 707	958 833 (60.35%)	398 761 (25.1%)	175 956 (11.08%)	55 157 (3.47%)
Channel 2	1 782 737	885 329 (49.66%)	429 968 (24.12%)	275 352 (15.45%)	192 088 (10.77%)
Channel 3	1 523 760	936 281 (61.45%)	481 397 (31.59%)	98 192 (6.44%)	7 890 (0.52%)
Single-photon	6 997 776	6 158 472 (88.01%)	809 273 (11.56%)	29 837 (0.43%)	194 (0%)

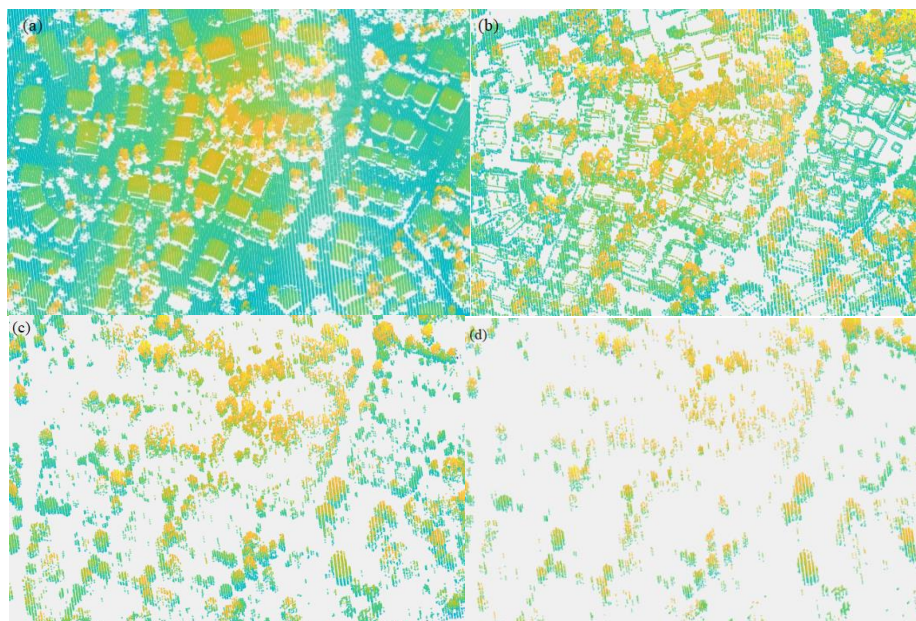


**Figure 8.** Echoes from channel 1 of multispectral Lidar.  
 (a) one echo; (b) two echoes; (c) three echoes; (d) four echoes.

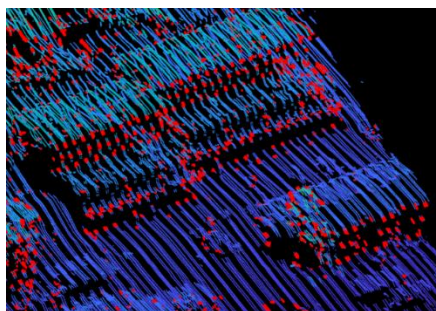


**Figure 9.** The points with three echoes from channel 3 overlapped with the point cloud of the scene.  
 The red points have three echoes from channel 3.

### 5.3. Comparison of the Data Intensity and Density

Fig. 10 shows the histogram of intensity of a scene from the multispectral and single-photon Lidar. The scene data (see Fig. 10 (e)) contain diverse objects e.g., buildings, trees, bushes, and ground, with an area of 0.18 km<sup>2</sup>. The intensity ranges from different channels of multispectral Lidar vary, for instance, 0~3999 in channel 1, 0~3814 in channel 2, 0~827 in channel 3, and 2266~14429 in single-photon data. The maximum values of the intensity data vary from different test areas. Despite different intensity ranges from the individual channel, in channel 1, 99.83% of points have intensity range in 0~150. In channel 2 and channel 3, they are 99.93% and 98.9%, respectively. It indicates that each channel of multispectral Lidar has the same scale of intensity despite different intensity ranges. Due to the intensity values of single-photon data in the form of pulse widths, the 'intensity values' become not comparable with the intensity values from multispectral data. In single-photon data, 99.16% of points have the 'intensity' values in 4000~11,000. Fig. 10 (f) exhibits the points with intensity values greater than 200 from each channel of multispectral Lidar. Points in blue are from channel 1. The red ones are from channel 2, and the green ones are from channel 3. These points are randomly distributed. The points with extremely high-intensity values can be the noise from the strong reflection by sunlight. Due to the different scan angles of each channel, these points are scattered. Also, the histogram distribution of intensity in multispectral Lidar is different from single-photon. The majority of the points from multispectral Lidar are located in a lower intensity area, while those from single-photon Lidar are located in a middle-intensity area. It is also evidenced by the fact that the 'intensity' in single-photon is different from the traditional Lidar system.

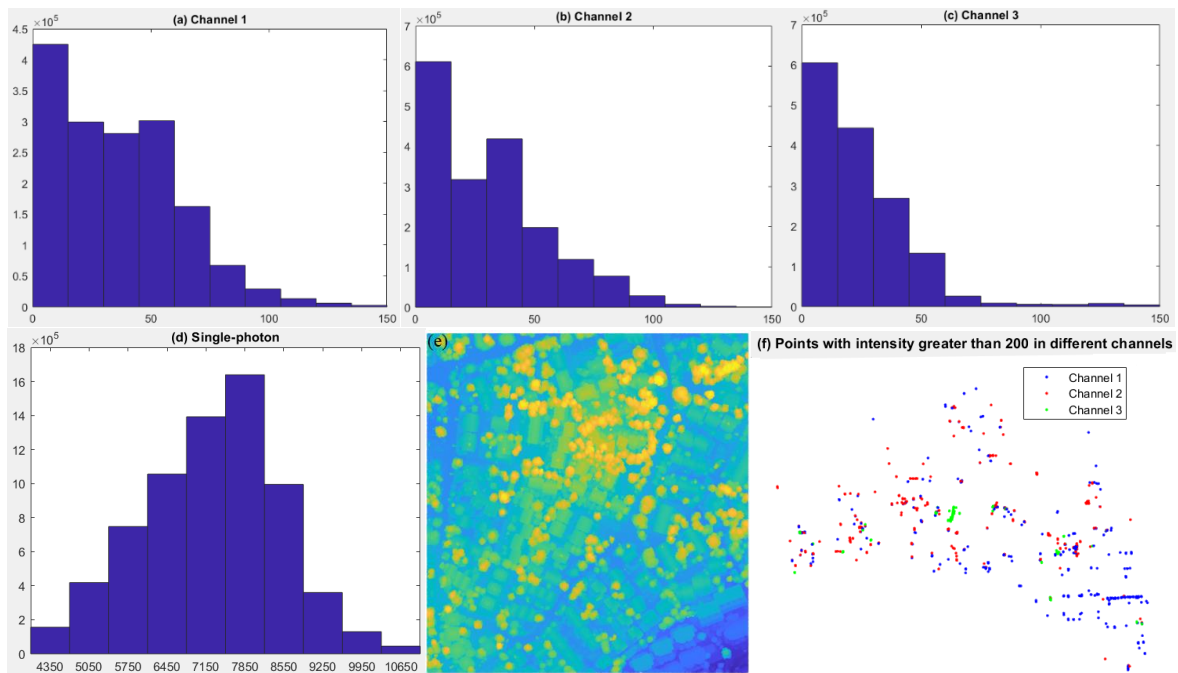


**Figure 10.** Histogram of the intensity of the scene data from multispectral and single-photon Lidar.

(a) channel 1: 1550nm, (b) channel 2: 1064nm, (c) channel 3: 532nm, (d) single-photon Lidar, (e) point cloud of the scene from channel 1, and (f) distribution of the points with intensity values greater than 200 in each channel of multispectral Lidar.

An example of using intensity as a threshold for object classification is demonstrated in Fig. 11. It is found that the green channel data can remove the vegetation simply by an intensity threshold. Here, the threshold is set to 18. Vegetation has a weaker intensity than the other objects. However, in the other two channels, by an intensity threshold, vegetation cannot be separated from the buildings.

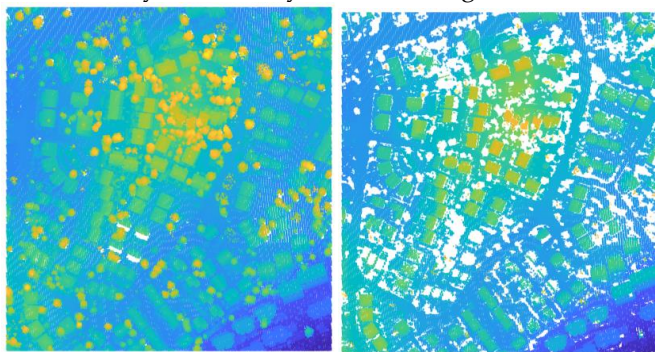


**Figure 11.** An example of the intensity for object classification (from the channel3 of multispectral Lidar). Left: original point cloud from channel 3; Right: a result after an intensity threshold (intensity >18)

Bakuła [8] utilized the tested point clouds with average densities of 25, 23, and 20 points/m<sup>2</sup> for the green (G), NIR, and SWIR lasers, respectively. The author claimed that “if a scene had a lot of vegetation, the points in NIR are relatively dense. When a shallow watery area, more dense points can be acquired from the green channel. In an urban area, more points are from the SWIR channel.”

However, according to our observations, there is no significant difference in the density of the points from each multispectral Lidar channel regarding the building data. There are fewer points in the combined multispectral Lidar data than in the single-photon Lidar data. In addition, the multispectral Lidar data are not evenly distributed. As a result, the corners of the roofs in an individual channel are not as accurate as those in the combined multispectral Lidar data. Single-photon Lidar data are much denser than the combined multispectral Lidar channel data, although the altitude of data acquisition of single-photon Lidar (3600 m) is higher than that of multispectral

Lidar (650m). The corners in the single-photon Lidar dataset are well defined. Fig. 12 shows the point distributions in the single-photon and multispectral Lidar datasets.

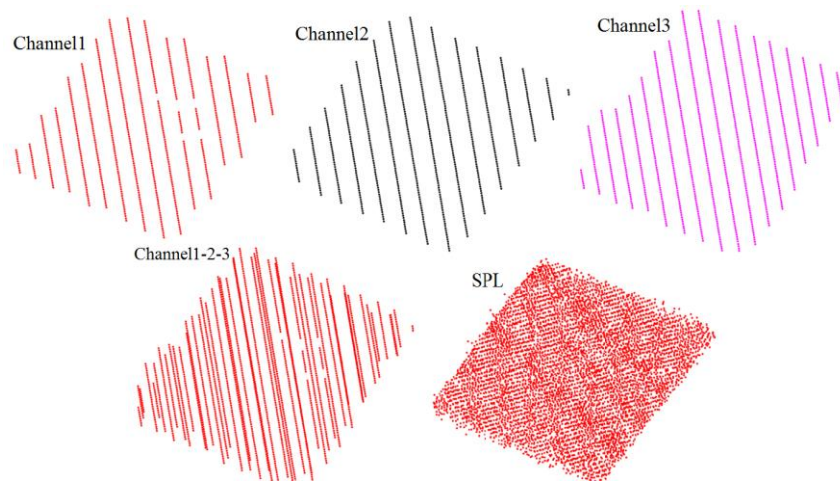


**Figure 12.** Example of the point distribution for a building roof from the different datasets: channel 1, channel 2, channel 3, the combination of channels 1, 2, and 3, and single-photon Lidar (SPL).

Table 3 shows the number of points from randomly selected building roofs. There is no evidence that one channel captures more building points than the other channels. The densities of building points vary across different buildings. For some roofs, channel 1 acquired more points than the other channels, while for the other four roofs, channel 3 obtained more points. For example, for roof 1, channel 2 obtained more points than the other channels, while for roof 2 and roof 3, channel 2 obtained the least number of points. This phenomenon can be caused by the interaction between the roof materials and the spectrum or the different viewing angles. When comparing the single-photon Lidar data with the multispectral Lidar data, the number of points from the single-photon Lidar data (with the test data) is approximately 1.5-1.9 times more than that from combined multispectral data.

**Table 3.** The number of points in the multispectral and single-photon Lidar data.

		Roof 1	Roof 2	Roof 3	Roof 4	Roof 5
		NoP	NoP	NoP	NoP	NoP
Multispectral Lidar	Channel 1	1142	618	1286	1191	1144
	Channel 2	1405	534	1251	1213	1457
	Channel 3	1121	756	1291	1365	1441
	Channel 1-2-3	3668	1908	3828	3769	4042
Single-photon Lidar		5553	3400	7467	7342	5562

\*NoP is the number of points on a building roof.

#### 5.4. Comparison of the Data Resolution/Level of Details and Data Defects

Figure 13 shows a building roof derived from the individual channels of the multispectral Lidar data, the combined multispectral Lidar data, and the single-photon Lidar data. The building eaves from the single-photon Lidar data are visible, but they are difficult to recognize in the individual channels of the multispectral Lidar data. The individual channels might suffer from building defects, while the fused multispectral Lidar data improve the completeness of the buildings. In general, the building from the single-photon Lidar data showed more details and better completeness than that from the multispectral Lidar data.



**Figure 13.** Building roof from the different datasets. From left to right: channel 1, channel 2, channel 3, channel combination, and single-photon Lidar data.

From the multispectral Lidar data, we found that while some buildings were missing in one channel, they were observed in another channel. This finding shows the complementary characteristics of the multispectral data and its potential for displaying material properties. We chose one area covering 152 buildings. The building roofs were selected from each channel. There were 16 buildings missing from channel 1, and six buildings had half roofs. In channel 2, the number of missed buildings was 35, and ten buildings had only half roofs. Channel 3 showed better results: only eight buildings were missing. The buildings partially shown might be caused by occlusions, e.g. from trees. Due to the difference of viewing angle of multispectral channels, it is possible that an object is occluded in one channel but it is visible in another channel. When one building is missing in one channel but it shows in another channel, it might be caused by the interaction between spectra and roof material.

There were four buildings lost from all the channels, but they were present in the single-photon Lidar dataset. The reason might be the different data acquisition times of the multispectral and single-photon Lidar data. The single-photon Lidar data were acquired later than the multispectral Lidar data. Thus, those four buildings can be considered new buildings in that area.

Figure 14 exhibits the data from channels of 1550nm, 1064nm, and 532nm. It can be seen that in channel 1550nm, some of the building roofs were partly captured, while they were completely acquired from the other two channels. It can be caused by different angles of scanning towards the scene and tree occlusions. The completeness of the roof data can be improved by data fusion of three channels.

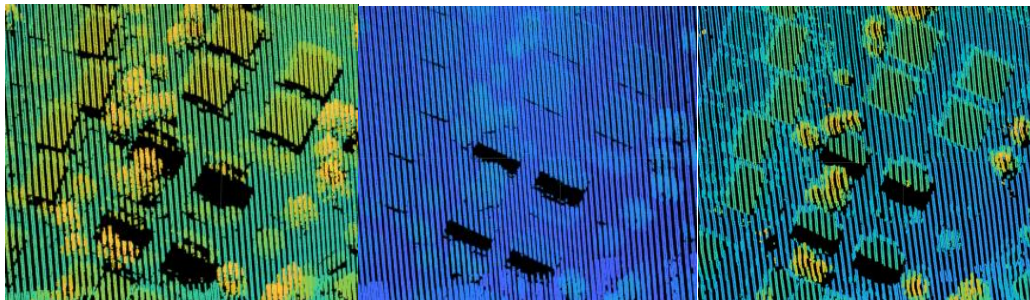


**Figure 14.** Examples of data defects from the different spectral channels.  
From left to right: 1550nm, 1064nm, and 532nm

### 5.5. Comparison of the Noise levels

Figure 15 shows the noise levels in the different datasets. It can be seen that single-photon Lidar produces more noise than the multispectral Lidar system. It can be interpreted that multiphoton thresholds in conventional Lidar have filtered out single-photon solar or dark count events, while single-photon Lidar accepts all solar and dark events. The solar count rate per pixel is proportional to the pixel field of view (FOV) and the receiver telescope aperture in single-photon Lidar. Thus, shrinking the pixel FOV reduces the solar count rate in single-photon Lidar data [30]. Therefore, the noise level in the single-photon data remains high.

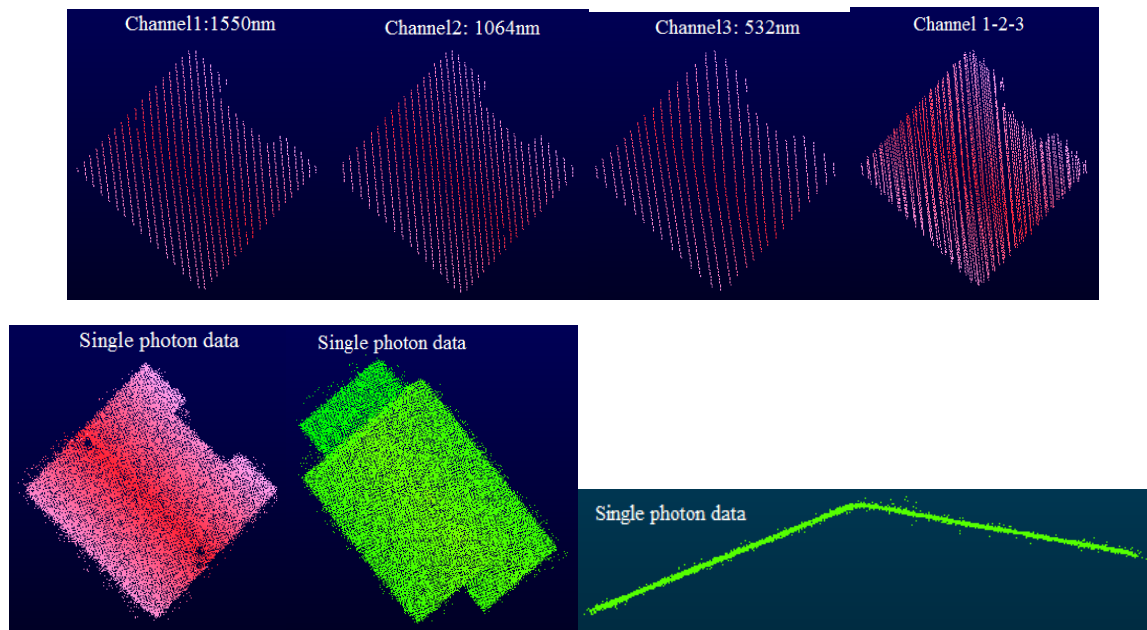


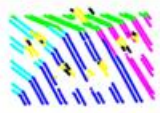
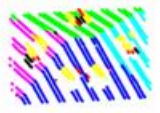
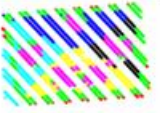
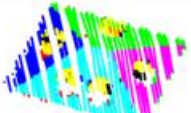
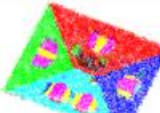
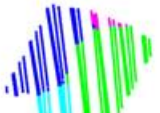
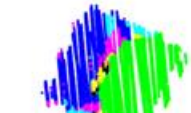
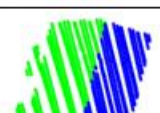
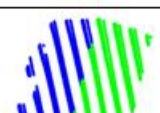
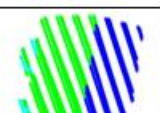
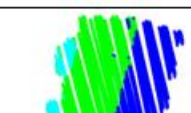
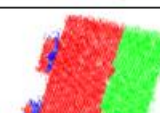
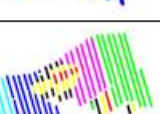
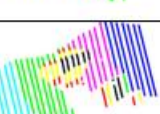
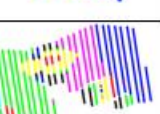
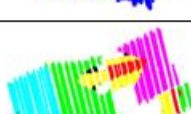
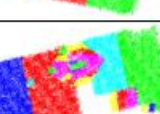
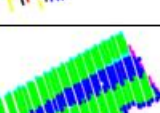
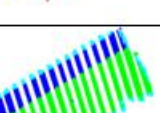
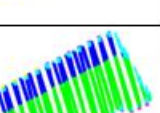
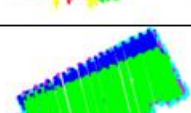
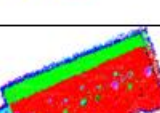
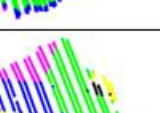
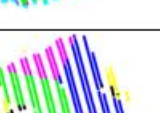
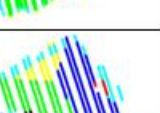
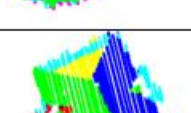
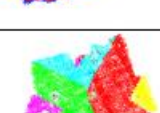
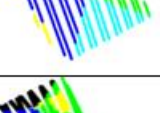
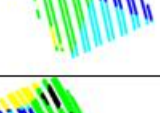
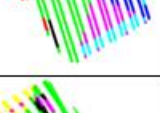
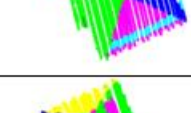
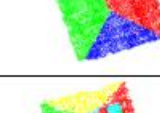
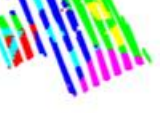
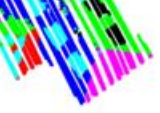
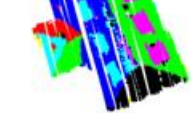
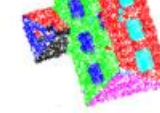
**Figure 15.** Noise level exhibition of different datasets.

### 5.6. Plane Detection

The planes were detected from the five datasets. Each dataset includes eight stylish building roofs with different complexities. Forty results were obtained (Table 4). For this plane detection test, the algorithm stops when the number of points is less than a threshold. For different datasets, we set thresholds according to their densities of points. We assume that if the rest points are less than  $2\text{m}^2$ , the algorithm stops. For the single-photon data with the point density of  $48\text{ points/m}^2$ , the threshold is 96. When the density of points is 8.5, the threshold is set to 17. The threshold for the distance from a point to the plane is 0.2m. It is the same for all datasets.

The density and distribution of points have a great effect on plane detection. Among all the datasets, the single-photon Lidar outperformed the others. The single-photon Lidar data show the most details of the building structure. Most of the planes were correctly detected from the single-photon Lidar dataset. Regarding the multispectral Lidar data, the combined data increased the details and completeness of the buildings compared to the individual-channel data. Due to the linear point distribution of the multispectral Lidar data, the spaces between the lines are visible, especially in the data from the individual channels. Thus, some details might be lost or incomplete, e.g., some eaves or other small parts of the building. The difference in plane detection between the individual channels is subtle. Regarding the building roof structure, B1 consists of four roof planes, five dormers, and two chimneys. All the components are present in the single-photon Lidar data. However, in the combined multispectral Lidar data, the two chimneys are not present. In the individual channel of multispectral Lidar data, except for the missed chimneys, the dormers are incomplete. In B3, two small eaves are clearly shown in the single-photon Lidar data, but they are not recognizable in the individual-channel data. B7 has eight dormers. They are well presented in the single-photon Lidar data. In the combined multispectral Lidar data, the dormers are not complete. In channel 1 and channel 3, they are worse. Only some of them are present. The planes detected from the channel 3 data are trivial due to the large space between the linear point distributions.

**Table 4.** Plane detection results.

	Channel 1	Channel 2	Channel 3	Channel_all	Single-photon
B1					
B2					
B3					
B4					
B5					
B6					
B7					
B8					

5.7. Comparison of the Building Data between the Multispectral and Single-Photon Lidar Data with the 3D Building Vector Data

The building point clouds from single-photon and multispectral Lidar datasets are compared with the reference building models. The distance of the point to the mesh is estimated. Each point of the compared point cloud searches the nearest triangle in the reference meshes. Fig. 16 shows the point cloud is overlapped with the building models. The point cloud is in blue while the building models are in gray.

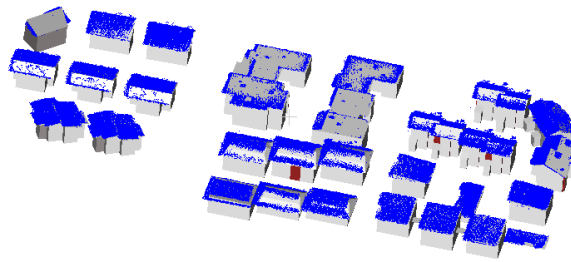


Figure 16. Lidar point cloud overlaps with reference data (3D building models)

Blue: point cloud, Gray: 3D building models

The left image of Fig. 17 shows that the building data from channel 1 have the smallest standard deviation, while the single-photon Lidar building data have the largest standard deviation. Regarding the multispectral Lidar data, the data from channel 1 have a smaller standard deviation than those from the other channels. Despite the largest deviation achieved by the single-photon Lidar data, these data have the smallest mean distance to the reference data. The data from channel 3 have the largest mean distance. However, the difference in the mean distances between channel 2 (0.126 m) and channel 3 (0.1279 m) is very small. From the above assessment can be seen that the accuracy of the datasets is quite close to each other (less than 0.08m). The accuracy of the single-photon data might be affected by multiple factors such as the flight height and noise presence, and so on.

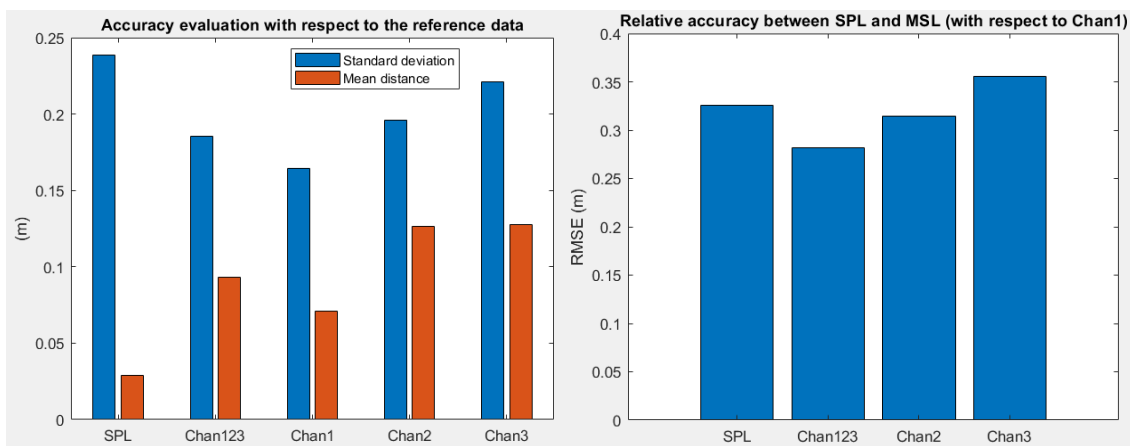


Figure 17. Accuracy Evaluation

Left: Accuracy evaluation with respect to the reference data; Right: Relative accuracy evaluation for the single-photon and multispectral Lidar data, with respect to channel 1.

Due to the smallest standard deviation in data from channel 1, we estimated the Root Mean Square Error (RMSE) for the single-photon and multispectral Lidar data, with respect to channel 1, by using the Iterative closest point algorithm (ICP). Thus, the evaluation does not rely on the accuracy of the reference data. For each point in the source point cloud, the closest point in the reference point cloud is searched. The right image of Fig. 17 shows the result of the relative accuracy evaluation with respect to channel 1. Their RMSE is 0.3257m, 0.2817m, 0.3145m, and 0.3559m, respectively for SPL, channel 123, channel 2, and channel 3. Channel 123 shows the smallest RMSE. Both accuracy evaluations indicate that the combined data from multispectral channels show better accuracy than the single-photon data. However, the difference is relatively small.

## 6. Discussion

### 6.1 The use of echo information for enhancing visual effects in residential areas

As mentioned in section 5.2, for most test data, buildings typically have one or two backscattered echoes. The vegetation, on the other hand, may have up to four echoes. The third and fourth echoes

are typically vegetation. Thus, we may exploit such echo information to enhance visualization. For example, the colors of the first and second echoes are plotted according to the height change while the third and fourth echoes are drawn in green. Thus, the buildings are easily distinguished from the surrounding trees. Fig. 18 takes a piece of data from channel 1 as an example. The left of the figure shows the point cloud. The colors are displayed according to the heights. The right of the figure shows the visual enhancement. The third and fourth echoes were plotted in green circles to enhance the vegetation presence. It can be seen that when using height information to display the data, it is a challenge to distinguish similar height buildings and trees. After visual enhancement, it is easy to interpret the spatial information of the scene.

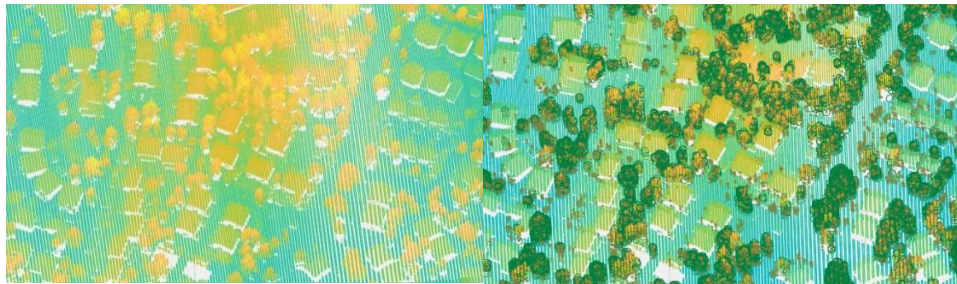


**Figure 18.** Visual enhancement by exploiting the echo information in multispectral data  
Left: visualize the data by using height information; Right: visual enhancement by using echo information (green color for the third and fourth echoes)

Fig. 19 demonstrates the visual enhancement using echoes information for single-photon data. The left image shows the scene with the color defined by the height. The right image exhibits the visual enhancement for the scene. It was plotted by a combination of different echoes: the first echo was plotted by the color defined by the height; the second echo was plotted by green dots; the third and fourth echoes were plotted by green circles.

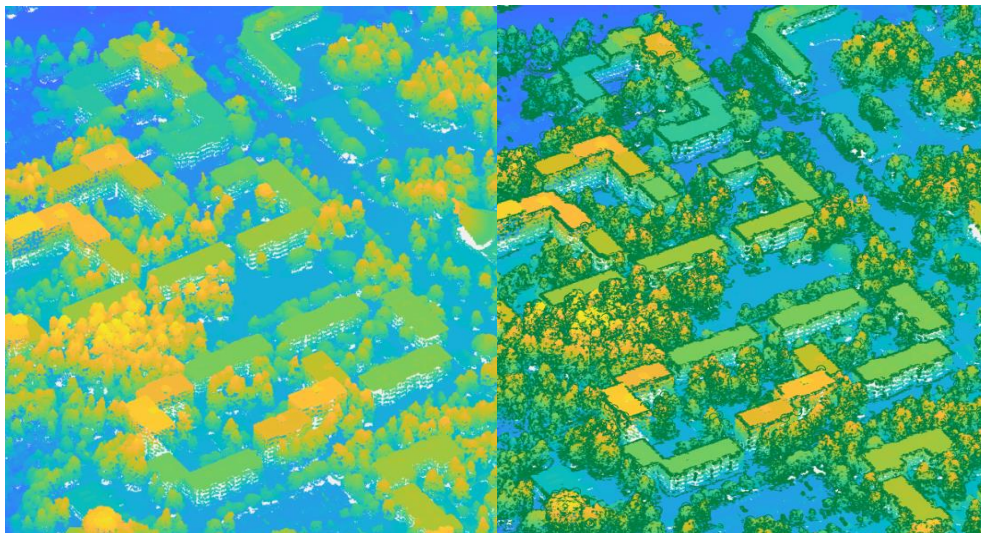


**Figure 19.** Visual enhancement by exploiting the echo information in single-photon data  
Left: visualize the data by using height information; Right: visual enhancement by using echo information (green color for the second, third, and fourth echoes)

From Fig. 18 and 19 demonstrations, it can be seen that for multispectral data, the visualization was enhanced by data with three and four echoes. While for single-photon data, it was not enough to utilize the data with three and four echoes. The data with the two echoes were also needed to improve scene visualization. It is because there were only 0.4% of single-photon data with three and four echoes.

## 6.2 An exploration of the possibility of using spectral information from multispectral data as colorful textures

We explored the intensity values in the spectrum of the multispectral Lidar dataset. The intensity information was exploited as textures of objects. Fig. 20 shows all combinations of intensity values as RGB information, with different orders. In total, there are six combinations. In the case of Figure 20a, for the combination of channel 213, the intensity values in channels 2, 1, and 3 are red, green, and blue, accordingly.

With different combinations of the intensity values, the building roofs are presented in different colors, and the entire scene becomes colorful. Additionally, the objects in the scene are easy to visually distinguish. The benefit of utilizing multispectral Lidar channel information for point cloud coloring is that it is independent of the lighting conditions, unlike commonly applied image-based colorization.

Fernandez-Diaz et. al [31] exhibited the false-color multispectral intensity image using the 1550 nm intensity for the red and the 1064 and 532 nm intensities for the green and blue or the blue and green. It is similar to the cases shown in Fig. 20 (b) and (d).

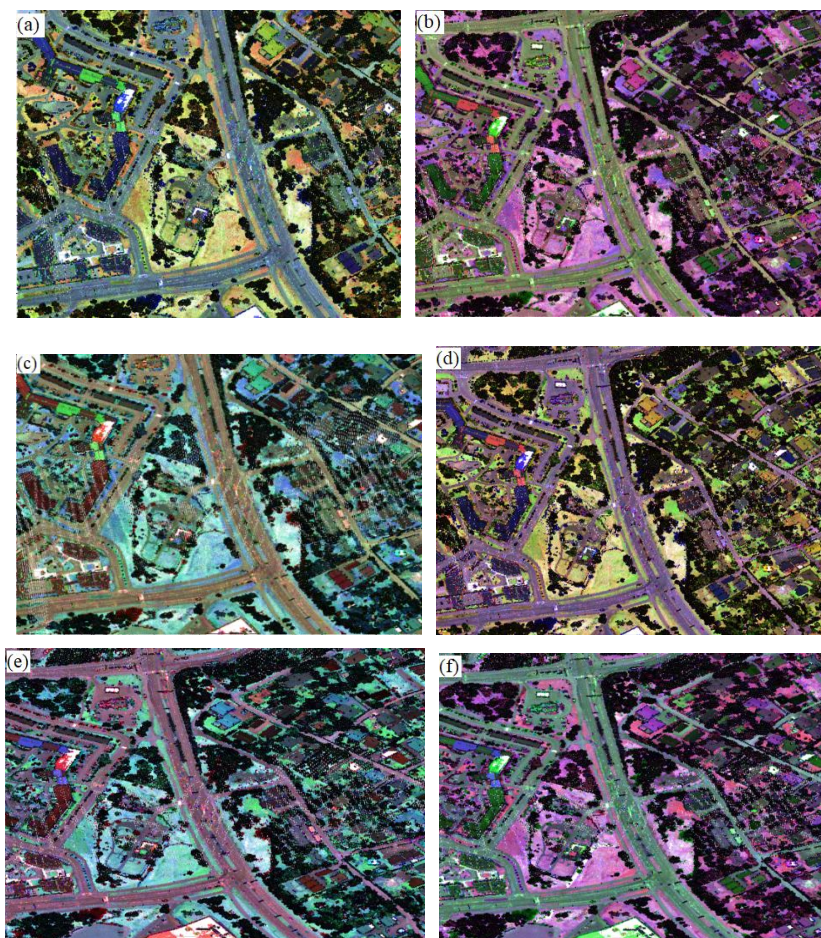


**Figure 20.** Combination of the intensity values from individual channels for the textures of a scene. The combination of different orders: (a) the combination of channels 2, 1, and 3; (b) the combination of channels 1, 3, and 2; (c) the combination of channels 3, 1, and 2; (d) the combination of channels 1, 2, and 3; (e) the combination of channels 3, 2, and 1; (f) the combination of channels 2, 3, and 1.

### 6.3 The advantages and disadvantages of multispectral and single-photon Lidar technologies and their applications in urban building environments

Currently, the main applications of Lidar building data include building detection/extraction, 3D city models, archeology, and 3D scene visualization. Compared to conventional Lidar, multispectral Lidar is beneficial for object classification due to its rich spectral information [10,16]. The complementarity between different spectra increases the building completeness. When some

information is absent in one channel, it might present in another channel. In archeology, Briese et al. [7] claimed that 1550 nm ALS data exhibited more detailed archeological features than those at wavelengths of 1064 nm and 532 nm. Therefore, multispectral data containing a wavelength of 1550 nm are beneficial in archeology. In addition, the coordinates of multispectral data can be used to reconstruct 3D geometric models; the spectral information can be used for texturing the scene. These 3D models can be visualized using different combinations of spectral textures. The point distribution of the multispectral data is not regular. Gaps exist between data lines, which might lead to the loss of information. Utilizing echo information to enhance the visual effects has been demonstrated in section 6.1. By plotting the points of the three and four echoes of multispectral data in green, the spatial information and their relations are easier to be visually interpreted. By employing the multispectral intensity information with different combinations, the scene can be textured with rich colors. By an assessment of multispectral data with respect to the reference data, it shows better accuracy than single-photon data.

Research on single-photon Lidar data is still in the very beginning stage. There is still much room for studying the use of these data, especially in applications related to building environments. Our study has revealed that single-photon Lidar data present high-density point clouds and small details, which are beneficial for 3D city modeling. The echoes information of single-photon data can be used for visual enhancement. It is beneficial for scene interpretation. However, building classification using the intensity values of single-photon Lidar might not work because single-photon Lidar can't obtain echo from each pulse. Thus, existing software might not work well for single-photon data when the intensity information is required. Also, echo information from single-photon Lidar is different from multispectral Lidar, 99.57% of points have one or two echoes. The power of penetration of a single-photon laser beamlet is relatively weak when compared to traditional Lidar due to the splitting of a single pulse into 10x10 beamlets. However, such characteristics have no effects on building data because the building data typically have one or two echoes. For vegetation study, it might become an interesting topic.

## 7. Conclusions

This paper studied buildings from multispectral and single-photon Lidar data. The study was focused on data acquisition geometry, echoes, density, intensity, level of detail, data defects, noise level, and planar detection for 3D reconstruction. Additionally, the absolute and relative accuracy was evaluated with respect to the reference building vectors and channel 1 of the multispectral data, respectively. By this study, our findings are:

- i) Single-photon data contain more building facade data than multispectral data regarding the high buildings. For the low buildings, building facades from both data are missing;
- ii) The number of echoes of buildings is different in different datasets. The building points have three echoes from the channel of 532nm, while ones from the other channels have only two echoes.
- iii) Echo information can be exploited for visual enhancement. It makes the scene easy to be interpreted;
- iv) By exploring the intensity data, it is found that in channel 3 of multispectral Lidar, vegetation and building roofs can be easily separated by an intensity threshold. However, it doesn't work for data from the other channels;
- v) Due to the high-density of single-photon Lidar data, it provides more details than multispectral Lidar data regarding buildings. Thus, it is more suitable for high detailed 3D city model;
- vi) It was evidenced that in multispectral data some buildings are missing in one channel but presenting in the other channel. Some buildings are partly shown in one channel but fully shown on another channel. Data combination from three channels increases the completeness of buildings;
- vii) It was observed that single-photon data contain more noise points than multispectral data.

For single-photon Lidar, due to high efficiency in data acquisition and high details in building roofs, the advantages of exploiting single-photon Lidar for large area 3D city models are evident.

**Author Contributions:** In this study, Lingli Zhu was responsible for the method development and testing, as well as for composing the manuscript. Juha Hyypä, Juho-Pekka Virtanen, and Xiaowei Yu gave writing advice. Harri Kaartinen acquired funding.

**Funding:** This research was funded by the Strategic Research Council at the Academy of Finland "Competence Based Growth Through Integrated Disruptive Technologies of 3D Digitalization, Robotics, Geospatial Information, and Image Processing/Computing - Point Cloud Ecosystem project (293389/314312)"

**Acknowledgments:** The City of Espoo is acknowledged for their support in providing the reference data for this study for free.

**Conflicts of Interest:** The authors declare no conflicts of interest.

## References

1. Pfennigbauer, M.; Ullrich, A. Multi-wavelength airborne laser scanning. In *Proceedings of the International Lidar Mapping Forum*; ILMF 2011: New Orleans, February 7-9, 2011.
2. Matikainen, L.; Karila, K.; Hyypä, J.; Litkey, P. Multispectral airborne laser scanning for automated map updating. In *Proceedings of the International Archives of the Photogrammetry, Remote Sensing and Spatial Information Sciences, Prague, Czech Republic, 12–19 July 2016*; ISPRS Congress: Prague, Czech Republic, ISPRS Congress, 2016, Volume XLI-B3, 2016, XXIII, pp. 323–330.
3. Optech. Titan multispectral lidar system. Available online: <https://www.teledyneoptech.com/en/home/> (accessed on 21 March 2019).
4. Degnan, J.J. Scanning, multibeam, single-photon lidars for rapid, large scale, high resolution, topographic and bathymetric mapping. *Remote Sens.* **2016**, *8*, 958; DOI:10.3390/rs8110958.
5. Charbon, E.; Regazzoni, F. Single-photon image sensors. In *Proceedings of the 50th Annual Design Automation Conference, San Francisco, CA, USA, 19–23 July 2013*; Association for Computing Machinery: Austin, Texas, 2013, pp. 1–4.
6. Hartzell, P.; Dang, Z.; Pan, Z.; Glennie, C. Radiometric evaluation of an airborne single-photon lidar sensor. *IEEE Geosci. Remote Sens. Lett.* **2018**, *15*, 1466–1470; DOI:10.1109/LGRS.2018.2841811.
7. Briese, C.; Pfennigbauer, M.; Ullrich, A.; Doneus, M. Multi-wavelength airborne laser scanning for archaeological prospection. *Int. Arch. Photogramm. Remote Sens. Spat. Inf. Sci.* **2013**, *40*, 119–124; DOI:10.5194/isprsarchives-XL-5-W2-119-2013.
8. Bakula, K. Multispectral airborne laser scanning-a new trend in the development of LiDAR technology. *Arch. Fotogram. Kartogr. Teledetekcji* **2015**, *27*, 25–44.
9. Wichmann, V.; Bremer, M.; Lindenberger, J.; Rutzinger, M.; Georges, C.; Petrini- Monteferrri, F. Evaluating the potential of multispectral airborne lidar for topographic mapping and land cover classification. *ISPRS Ann. Photogram. Remote Sens. Spat. Inform. Sci.* **2015**, *II-3/W5*, 113–119; DOI:10.5194/isprsannals-II-3-W5-113-2015.
10. Gong, W.; Sun, J.; Shi, S.; Yang, J.; Du, L.; Zhu, B.; Song, S. Investigating the potential of using the spatial and spectral information of multispectral LiDAR for object classification. *Sensors (Basel)* **2015**, *15*, 21989–22002; DOI:10.3390/s150921989.
11. Ekhtari, N.; Glennie, C.; Fernandez-Diaz, J.C. Classification of airborne multispectral lidar point clouds for land cover mapping. *IEEE J. Sel. Top. Appl. Earth Obs. Remote Sens.* **2018**, *11*, 2068–2078; DOI:10.1109/JSTARS.2018.2835483.
12. Hopkinson, C.; Chasmer, L.; Gynan, C.; Mahoney, C.; Sitar, M. Multisensor and multispectral lidar characterization and classification of a forest environment. *Can. J. Remote Sens.* **2016**, *42*, 501–520; DOI:10.1080/07038992.2016.1196584.
13. Kukkonen, M.; Maltamo, M.; Korhonen, L.; Packalen, P. Comparison of multispectral airborne laser scanning and stereo matching of aerial images as a single sensor solution to forest inventories by tree species. *Remote Sens. Environ.* **2019**, *231*, 111208; DOI:10.1016/j.rse.2019.05.027.
14. Matikainen, L.; Karila, K.; Hyypä, J.; Litkey, P.; Puttonen, E.; Ahokas, E. Object-based analysis of multispectral airborne laser scanner data for land cover classification and map updating. *ISPRS J. Photogramm. Remote Sens.* **2017**, *128*, 298–313; DOI:10.1016/j.isprsjprs.2017.04.005.
15. Yan, W.Y.; Shaker, A.; LaRocque, P.E. Water mapping using multispectral airborne LiDAR data. *Int. Arch. Photogramm. Remote Sens. Spat. Inf. Sci.* **2018**, 2047–2052; DOI:10.5194/isprs-archives-XLII-3-2047-2018.

16. Karila, K.; Matikainen, L.; Puttonen, E.; Hyypä, J. Feasibility of multispectral airborne laser scanning data for road mapping. *IEEE Geosci. Remote Sens. Lett.* **2017**, *14*, 294–298; DOI:10.1109/LGRS.2016.2631261.
17. Morsy, S., Shaker, A. and El-Rabbany, A., 2017. Multispectral LiDAR data for land cover classification of urban areas. *Sensors*, *17*(5), p.958.
18. Shaker, A., Yan, W.Y. and LaRocque, P.E., 2019. Automatic land-water classification using multispectral airborne LiDAR data for near-shore and river environments. *ISPRS journal of photogrammetry and remote sensing*, *152*, pp.94-108.
19. Stoker, J.M.; Abdullah, Q.A.; Nayegandhi, A.; Winehouse, J. Evaluation of single photon and Geiger mode LiDAR for the 3D elevation program. *Remote Sens.* **2016**, *8*, 767; DOI:10.3390/rs8090767.
20. Swatantran, A.; Tang, H.; Barrett, T.; DeCola, P.; Dubayah, R. Rapid, high-resolution forest structure and terrain mapping over large areas using single photon lidar. *Sci. Rep.* **2016**, *6*, 28277; DOI:10.1038/srep28277.
21. Tang, H.; Swatantran, A.; Barrett, T.; DeCola, P.; Dubayah, R. Voxel-based spatial filtering method for canopy height retrieval from airborne single-photon LiDAR. *Remote Sens.* **2016**, *8*, 771; DOI:10.3390/rs8090771.
22. Jutzi, B. Less photons for more LiDAR? A review from multi-photon-detection to single-photon-detection. In *Proceedings of the 56th Photogrammetric Week (PhoWo 2017), University of Stuttgart, September 11-15, 2017*; PhoWo: Stuttgart, Germany, 2017, pp. 6–S.
23. Mandlbürger, G.; Jutzi, B. Feasibility investigation on single photon lidar based water surface mapping. *ISPRS Ann. Photogramm. Remote Sens. Spat. Inf. Sci.* **2018**, *IV-1*, 109–116; DOI:10.5194/isprs-annals-IV-1-109-2018.
24. Matikainen, L., Karila, K., Litkey, P., Ahokas, E. and Hyypä, J., 2020. Combining single photon and multispectral airborne laser scanning for land cover classification. *ISPRS Journal of Photogrammetry and Remote Sensing*, *164*, pp.200-216.
25. Mandlbürger, G., Lehner, H. and Pfeifer, N., 2019. A COMPARISON OF SINGLE PHOTON AND FULL WAVEFORM LIDAR. *ISPRS Annals of Photogrammetry, Remote Sensing & Spatial Information Sciences*, *4*.
26. The NLS. The national land of Finland. Available online: <https://kartta.paikkatietoikkuna.fi/> (accessed on 15 August 2019).
27. Roncat, A., Wagner, W., Melzer, T., & Ullrich, A. (2008). Echo detection and localization in full-waveform airborne laser scanner data using the averaged square difference function estimator.
28. Brown, R., Hartzell, P. and Glennie, C., 2020. Evaluation of SPL100 Single Photon Lidar Data. *Remote Sensing*, *12*(4), p.722.
29. Torr, P.H.; Zisserman, A. MLESAC: A new robust estimator with application to estimating image geometry. *Comput. Vis. Image Underst.* **2000**, *78*, 138–156; DOI:10.1006/cviu.1999.0832.
30. Degnan, J.J. Photon-counting multikilohertz microlaser altimeters for airborne and spaceborne topographic measurements. *J. Geodyn.* **2002**, *34*, 503–549; DOI:10.1016/S0264-3707(02)00045-5.
31. Fernandez-Diaz, J.C., Carter, W.E., Glennie, C., Shrestha, R.L., Pan, Z., Ekhtari, N., Singhania, A., Hauser, D. and Sartori, M., 2016. Capability assessment and performance metrics for the Titan multispectral mapping lidar. *Remote Sensing*, *8*(11), p.936.